A complex containing the *O*-GlcNAc transferase OGT-1 and the ubiquitin ligase EEL-1 regulates GABA neuron function

Received for publication, January 7, 2019, and in revised form, March 7, 2019 Published, Papers in Press, March 11, 2019, DOI 10.1074/jbc.RA119.007406

Andrew C. Giles[‡], Muriel Desbois[‡], Karla J. Opperman[‡], Rubens Tavora[§], Marissa J. Maroni[‡], and Brock Grill[‡1]

From the [‡]Department of Neuroscience, The Scripps Research Institute, Scripps Florida, Jupiter, Florida 33458 and the [§]Harriet L. Wilkes Honors College, Florida Atlantic University, Jupiter, Florida 33458

Edited by Gerald W. Hart

Inhibitory GABAergic transmission is required for proper circuit function in the nervous system. However, our understanding of molecular mechanisms that preferentially influence GABAergic transmission, particularly presynaptic mechanisms, remains limited. We previously reported that the ubiquitin ligase EEL-1 preferentially regulates GABAergic presynaptic transmission. To further explore how EEL-1 functions, here we performed affinity purification proteomics using *Caenorhabditis elegans* and identified the *O*-GlcNAc transferase OGT-1 as an EEL-1 binding protein. This observation was intriguing, as we know little about how OGT-1 affects neuron function. Using *C. elegans* biochemistry, we confirmed that the OGT-1/EEL-1 complex forms in neurons *in vivo* and showed that the human orthologs, OGT and HUWE1, also bind in cell culture. We observed that, like EEL-1, OGT-1 is expressed in GABAergic motor neurons, localizes to GABAergic presynaptic terminals, and functions cell-autonomously to regulate GABA neuron function. Results with catalytically inactive point mutants indicated that OGT-1 glycosyltransferase activity is dispensable for GABA neuron function. Consistent with OGT-1 and EEL-1 forming a complex, genetic results using automated, behavioral pharmacology assays showed that *ogt-1* and *eel-1* act in parallel to regulate GABA neuron function. These findings demonstrate that OGT-1 and EEL-1 form a conserved signaling complex and function together to affect GABA neuron function.

GABA neurons are a critical component of nervous systems across the animal kingdom from mammals (1, 2) to simple invertebrates, such as *Caenorhabditis elegans* (3, 4). They provide essential inhibitory activity within neural circuits. In humans, various dysfunctions in GABA neurons and the imbalance between excitatory and inhibitory neurotransmission contribute to neurodevelopmental disorders (5, 6). Thus, understanding how GABA neuron function is regulated is critical for our understanding of nervous system function and disease.

This work was supported by NINDS, National Institutes of Health, Grant R01 NS072129 (to B. G.). The authors declare that they have no conflicts of interest with the contents of this article. The content is solely the responsibility of the authors and does not necessarily represent the official views of the National Institutes of Health.

This article contains Tables S1 and S2 and Figs. S1–S8.

[1] To whom correspondence should be addressed: Dept. of Neuroscience, The Scripps Research Institute, Scripps Florida, 130 Scripps Way, Jupiter, FL 33458. Tel.: 561-228-2110; Fax: 561-228-2111; E-mail: bgrill@scripps.edu.

Much remains unknown about molecular mechanisms that preferentially affect GABAergic transmission. Core presynaptic machinery, such as synaptotagmin, the SNARE complex, and active zone proteins, influence both glutamatergic and GABAergic transmission (7, 8). A few post-synaptic regulators that preferentially or specifically affect GABAergic transmission are known, including Gephyrin, Neuroligin2, Slitrk3, and GARHLs (9–13). In mammals, less is known about presynaptic GABA-specific regulators, but some proteins, such as synapsins, can differentially impact inhibitory transmission compared with excitatory transmission (14, 15).

In *C. elegans*, core presynaptic components play conserved roles in neurotransmission in the motor circuit, a model circuit with balanced excitatory cholinergic and inhibitory GABAergic neuron function (4, 16). Like mammals, relatively few proteins are known that preferentially regulate presynaptic GABA function in *C. elegans*. Nonetheless, the worm motor circuit has proven valuable for identifying molecules that regulate GABA neuron function. Examples include the NPR-1 neuropeptide Y receptor, the SEK-1 MAP2K, the F-box protein MEC-15, and the anaphase-promoting complex (17–19).

Recently, we showed the HECT family ubiquitin ligase EEL-1 (enhancer of EfL-1) is expressed broadly in the nervous system but preferentially affects GABAergic presynaptic transmission in the motor circuit of *C. elegans* (20). At present, it is unknown how EEL-1 regulates GABAergic presynaptic transmission. Our interest in exploring this question was heightened by extensive genetic links between the EEL-1 ortholog HUWE1 (HECT, UBA, and WWE domains containing protein 1) and intellectual disability. These include *HUWE1* copy number increases (21) and missense loss-of-function mutations that cause Juberg-Marsidi-Brooks syndrome and non-syndromic X-linked intellectual disability (20, 22, 23).

To determine how EEL-1 regulates GABAergic transmission, we performed affinity purification proteomics using *C. elegans* to identify EEL-1 binding proteins. The most prominent EEL-1 binding protein we identified was OGT-1 (*O*-linked β-*N*-acetylglucosamine (*O*-GlcNAc) transferase 1), a conserved glycosyltransferase that modifies protein function in the cytosol, nucleus, and mitochondria (24–26).

In mammals, OGT is expressed in the brain and localizes to presynaptic terminals (27, 28). Despite prominent OGT-mediated *O*-GlcNAcylation of synaptic proteins (29), the functional effects of OGT in the nervous system have only recently begun to be explored. OGT regulates mitochondrial motility in neu-

rons (30) and has been implicated in neurodegenerative disease (31). In OGT conditional knockout mice, AgRP (agouti-related protein) and PVN (paraventricular nucleus) neurons are functionally impaired, leading to impacts on fat metabolism and feeding behavior, respectively (32, 33). While glycosyltransferase activity is the most widely studied OGT activity, a much smaller body of work indicates that OGT can also act as a scaffold protein (25). At present, it is unknown whether this transferase-independent function of OGT has a role in the nervous system.

To explore the biological relationship between OGT-1 and EEL-1, we expanded upon our proteomic finding that OGT-1 was a putative EEL-1 binding protein with several independent experimental approaches. We biochemically validated the interaction between OGT-1 and EEL-1 and showed that it occurs in *C. elegans* neurons *in vivo*. Importantly, this interaction was conserved as it also occurred between HUWE1 and OGT, the orthologous human proteins. Similar to EEL-1, OGT-1 was broadly expressed in the nervous system, including the cholinergic and GABAergic neurons of the motor circuit, and localized to presynaptic terminals in GABA neurons. Results from genetic analysis using an automated behavioral assay and pharmacological manipulation of the motor circuit showed that OGT-1 affects GABA neuron function. Similar phenotypic defects in GABA neuron function were previously observed in *eel-1* mutants (20). Furthermore, genetic results indicate that OGT-1 functions in parallel to EEL-1 in GABA neurons. Consistent with this, OGT-1 and EEL-1 also act in parallel to affect locomotion. Findings with point mutations that impair catalytic activity show that OGT-1 functions independently of glycosyltransferase activity to affect GABA neuron function, whereas EEL-1 ubiquitin ligase activity is required. Thus, our study reveals the discovery of an OGT-1/EEL-1 protein complex that regulates GABA neuron function and provides the first evidence of a nonenzymatic OGT-1 function in the nervous system.

Results

Measuring C. elegans motor circuit function using an automated aldicarb assay

Previously, we used a combination of electrophysiology and behavioral pharmacology to show that EEL-1 regulates GABAergic presynaptic transmission (20). To determine how EEL-1 regulates GABA transmission, we wanted to use affinity purification proteomics to identify EEL-1 binding proteins. As the first step in this process, we developed an automated platform for evaluating motor circuit function using aldicarb pharmacology. Once established, this assay would allow us to rapidly and quantitatively evaluate whether EEL-1 reagents are functional *in vivo* and suitable for affinity purification proteomics.

The *C. elegans* motor circuit is composed of excitatory cholinergic and inhibitory GABAergic motor neurons that innervate body wall muscles to control contraction and relaxation, respectively (Fig. 1*A*). This balance of excitation and inhibition allows for coordinated sinusoidal movement of the body. A traditional pharmacological assay for assessing motor circuit function relies upon aldicarb, an inhibitor of acetylcholine esterase (AchE).[2] By impairing AchE, aldicarb causes accumulation of Ach over time, which leads to excess muscle contraction and gradual paralysis (Fig. 1*A*). Traditionally, this is measured by assessing *C. elegans* paralysis while animals are on agar plates containing aldicarb. Aldicarb-induced paralysis on plates is usually assessed manually, but it has been automated (34, 35). We developed an automated, liquid assay that uses MWT (Multi-Worm Tracker) to evaluate locomotion and aldicarb-induced paralysis (Fig. 1*B*). We simultaneously monitored 20 wells with 4 worms/well (Fig. 1*B*). We recorded 10 min of baseline movement, added a desired aldicarb dose, and recorded animal speed in response to drug. As expected, WT animals showed dose-dependent paralysis after aldicarb treatment (Fig. 1*C*). Compared with our experience with manual aldicarb assays on agar plates (20), this automated liquid assay increases throughput and has a large dynamic range that facilitates dose response analysis.

Mutants that have disrupted motor circuit function have altered aldicarb sensitivity (17, 34). Mutants with impaired cholinergic function accumulate Ach more slowly at the synapse when treated with aldicarb, which results in slower paralysis and resistance to aldicarb compared with WT animals. This is also the case for mutants that affect cholinergic and GABAergic function equally. There are two scenarios that lead to aldicarb resistance. The first is mutants with increased cholinergic function. The second is mutants that have preferentially disrupted inhibitory GABA function, which results in loss of relaxation and faster paralysis in the presence of aldicarb (Fig. 1*A*).

To assess the performance of our automated aldicarb assay, we tested several aldicarb hypersensitive mutants: hypersensitive mutants with increased cholinergic transmission (*goa-1* and *slo-1*), mutants that are defective in GABA biosynthesis (*unc-25*), and mutants that lack a GABA receptor subunit (*unc-49*) (17, 36). We also evaluated *eel-1 (zu462)* deletion mutants, which we previously showed are hypersensitive to aldicarb due to defects in GABAergic presynaptic transmission (20). Consistent with prior studies, these mutants were hypersensitive in automated aldicarb assays (Fig. 1*D* and Figs. S1 and S2*A*). Hypersensitivity in *eel-1* mutants was rescued by an integrated transgene that expressed EEL-1 using the native *eel-1* promoter (Fig. 1*D* and Fig. S2*A*). It is unclear why the EEL-1 transgene did not fully rescue. This could be because the *eel-1* promoter we designed is not ideal for EEL-1 expression, or EEL-1 is not expressed at optimal levels by the integrated multicopy transgene we used. Nonetheless, these results indicate that we have developed an automated liquid aldicarb assay that rapidly and quantitatively assesses motor circuit function. This approach allowed us to assess aldicarb hypersensitivity and rescue in *eel-1* mutants. Thus, this assay is suitable for

[2] The abbreviations used are: AchE, acetylcholinesterase; Ach, acetylcholine; IP, immunoprecipitation; NMJ, neuromuscular junction; FDR, false discovery rate; LSD, least significant difference; ANOVA, analysis of variance.

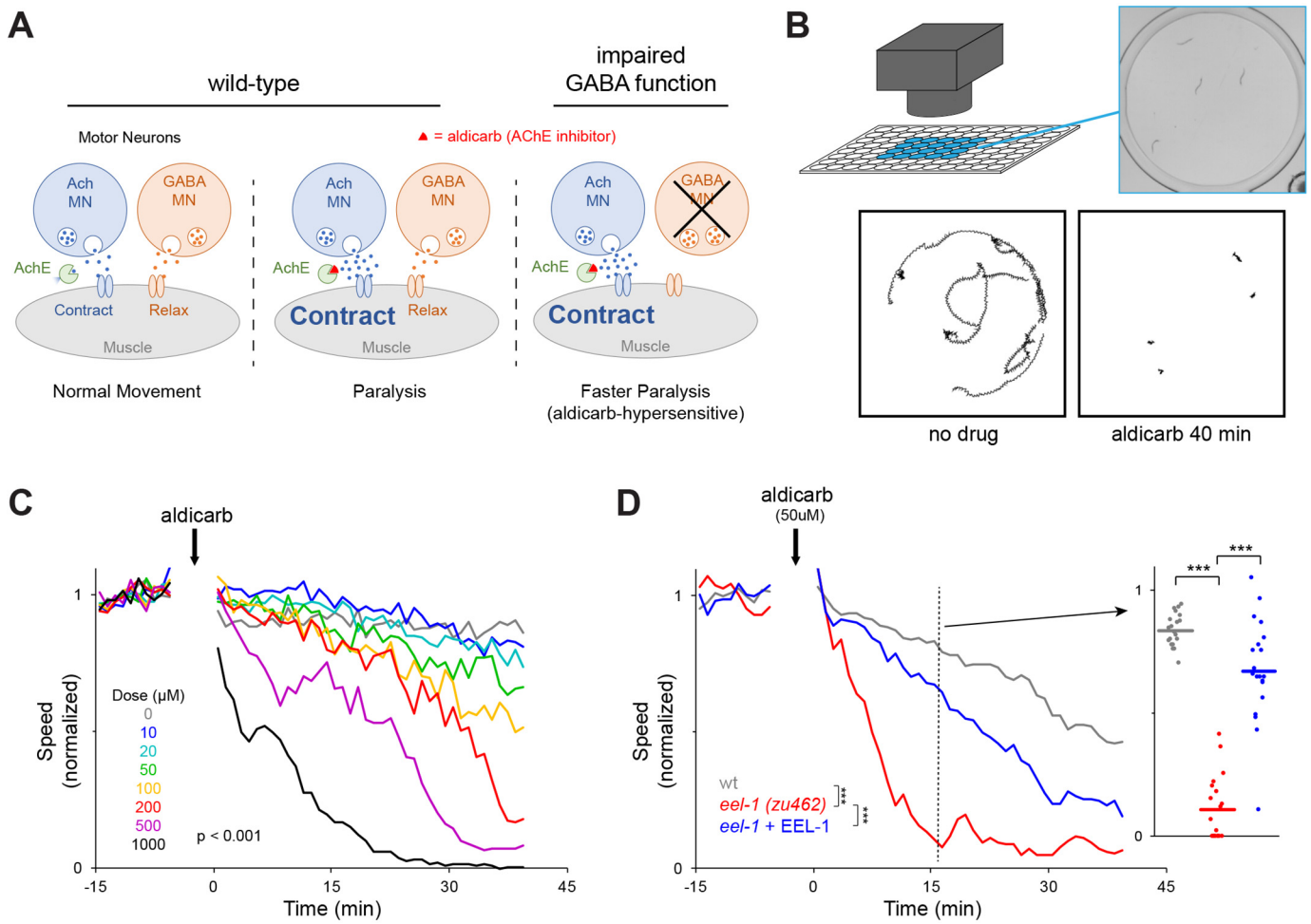

Figure 1. Automated behavioral assay shows that *eel-1* mutants are hypersensitive to aldicarb. *A*, depicted is the *C. elegans* motor circuit composed of excitatory cholinergic and inhibitory GABAergic motor neurons. Balance of contraction and relaxation is required for normal movement (*left*). Application of aldicarb, an AchE inhibitor, leads to excess cholinergic transmission and paralysis (*middle*). Mutants with impaired GABAergic transmission, such as *eel-1*, are hypersensitive to aldicarb and paralyze faster (*right*). *B*, schematic showing automated aldicarb assay with MWT. 20 wells are monitored simultaneously. Shown is an image of a single well with four animals (*right*). MWT plots depict animal swimming over a 1-min timeframe with and without aldicarb treatment (*below*). *C*, MWT analysis of aldicarb dose response for WT animals. Shown is the mean of multiple wells for each dose (n = 5–20 wells/dose); significance was determined using two-way ANOVA (dose *versus* time). *D*, *eel-1 (zu462)* mutants are hypersensitive to aldicarb, and transgenic expression of EEL-1 rescues aldicarb hypersensitivity. Shown are means (n = 20 wells/genotype). *Inset*, mean speed (*line*) and speed in each well (*circles*) at the indicated time for each genotype. Comparisons between genotypes represent pairwise two-way ANOVAs. Comparisons in the *inset* represent Fisher's LSD post hoc test (see Fig. S2*A* for further statistical analysis). ***, $p < 0.001$.

functional evaluation of EEL-1 constructs used for proteomics.

Functional assessment of EEL-1 affinity purification proteomic reagents

The next step toward EEL-1 affinity purification proteomics was to generate an *eel-1* protein null allele and evaluate this mutant in automated aldicarb assays. A protein null allele is particularly important to ensure that transgenic EEL-1 used for affinity purification proteomics is not competing with endogenous EEL-1 protein or EEL-1 fragments. We generated *bgg1*, an *eel-1* protein null, using Mos1-mediated deletion to eliminate the entire *eel-1* coding sequence, including the HECT ubiquitin ligase domain (Fig. 2, *A* and *B*). Importantly, *eel-1* (*bgg1*) mutants were hypersensitive to aldicarb (Fig. 2*C*), similar to *eel-1 (zu462)* mutants (Fig. 1*D*).

Next, we used automated aldicarb assays to evaluate rescue for EEL-1 constructs tagged with affinity purification tags. Several transgenes were generated that fused different constructs to a GS (protein G and streptavidin-binding protein) tag. GS was fused to WT EEL-1 or EEL-1 point-mutated at a critical residue (*C4144A*) required for E3 ubiquitin ligase activity (Fig. 2*B*) (37). We refer to the catalytically inactive point mutant as EEL-1 LD (ligase-dead). GS-tagged GFP served as a negative control. All transgenes were driven by the native *eel-1* promoter and expressed in the *eel-1 (bgg1)* protein null background. There were two reasons we included the EEL-1 LD transgene: 1) it remains unclear whether EEL-1 effects on aldicarb sensitivity and GABA transmission are mediated by EEL-1 ubiquitin ligase activity, and 2) we wanted to evaluate whether the EEL-1 LD can biochemically "trap" and enrich EEL-1 ubiquitination substrates in proteomic experiments.

As shown in Fig. 2*C*, GS::EEL-1 significantly rescued aldicarb hypersensitivity of *eel-1 (bgg1)* mutants. Similar to untagged EEL-1 (Fig. 1*D*), GS::EEL-1 only partially rescued *eel-1*. In contrast, rescue was not observed with GS::EEL-1

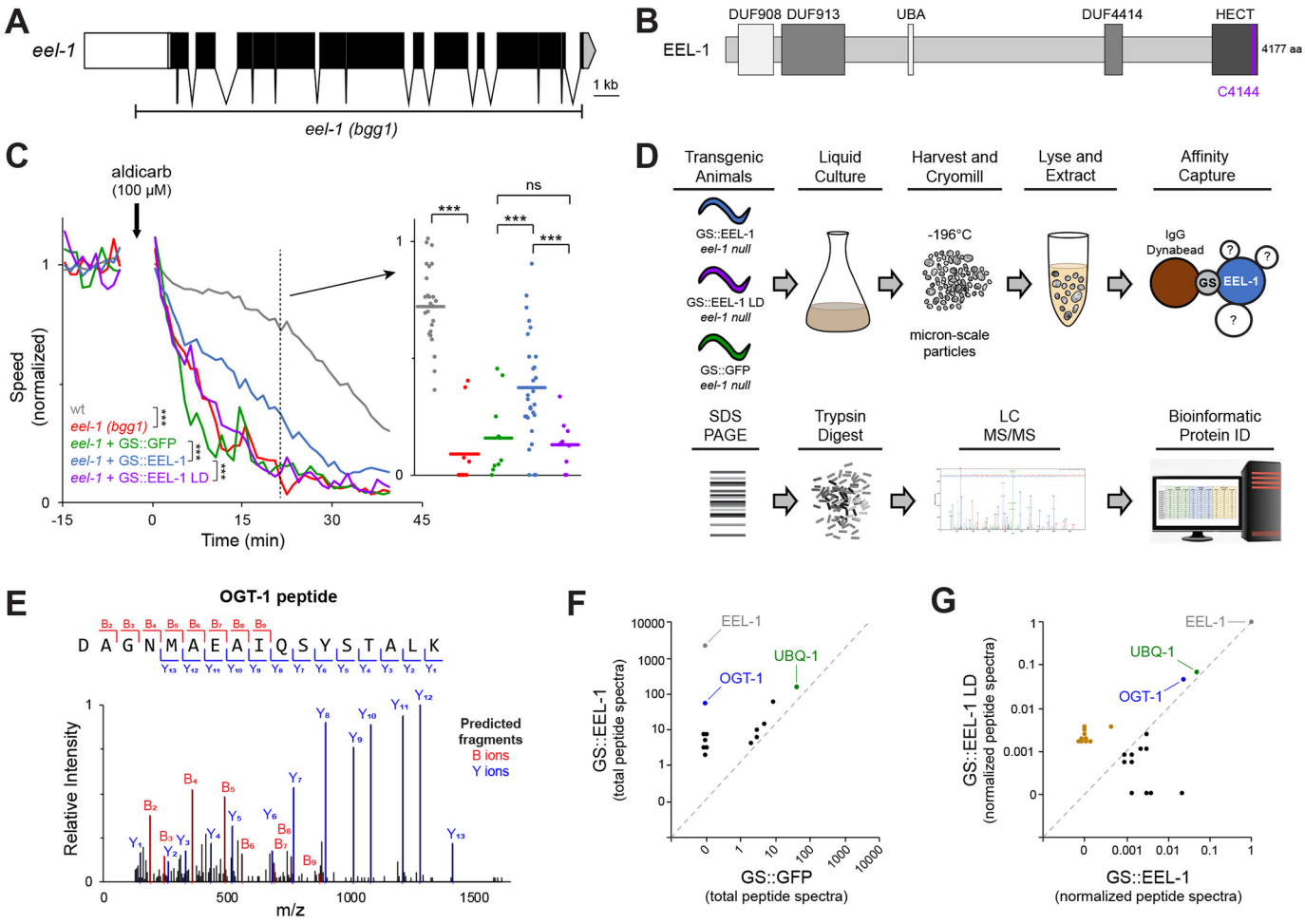

H

	Protein Identified	Vertebrate Homolog	MW (kDa)	Total Exp. #	Total Peptide Spectra			Total Peptide Spectra - Normalized						
					GS::GFP (Control)	GS::EEL-1	GS::EEL-1 LD	GS::GFP (Control)	GS::EEL-1	GS::EEL-1 LD	Fold increase GS::EEL-1 LD /GS::EEL-1	P-value GS::EEL-1 vs GS::GFP	P-value GS::EEL-1 LD vs GS::GFP	P-value GS::EEL-1 LD vs GS::EEL-1
Purification Target	EEL-1	HUWE1	465	4	0	2189	3763	0	1	1	1 x	-	-	-
Putative EEL-1 Binding Protein	UBQ-1	Ubiquitin	9	4	43	155	298	0	0.051	0.068	1.32 x	0.002	0.001	0.093 (ns)
	OGT-1	OGT	128	4	0	54	169	0	0.025	0.045	1.82 x	0.004	0.012	0.625 (ns)

Figure 2. Affinity purification proteomics from *C. elegans* identifies OGT-1 as a putative EEL-1 binding protein. *A*, schematic of *eel-1* gene and *eel-1* (*bgg1*) null allele generated by MosDel. Shown are exons (*black*), promoter (*white*), UTRs (*gray*), and introns (*gaps connected* by *lines*). *B*, schematic of EEL-1 protein with annotated domain of unknown function (*DUF*), ubiquitin-associated domain (*UBA*), and HECT ubiquitin ligase domain (*HECT*). *Highlighted* is the residue required for catalytic activity (*purple*). *C*, automated aldicarb assay showing that *eel-1* (*bgg1*) null mutants are hypersensitive to aldicarb compared with WT. Aldicarb hypersensitivity is rescued by GS::EEL-1 but not GS::EEL-1 LD. GS::GFP is negative control. Shown are means of multiple wells for each genotype ($n = 10–30$ wells with 4 worms/well). The *inset* shows mean speed (*line*) and individual data points at the indicated time. *D*, work flow for affinity purification proteomics from *C. elegans*. *E*, example of LC-MS/MS spectrum identifying OGT-1 peptide sequence from GS::EEL-1 sample. *F*, comparison of total peptide spectra from four proteomic experiments for proteins identified in GS::EEL-1 sample compared with GS::GFP sample. The *dashed line* denotes 2× enrichment above GS::GFP negative control. *G*, comparison of normalized total peptide spectra from four proteomic experiments for GS::EEL-1 LD compared with GS::EEL-1. *Highlighted* in *gold* are proteins found exclusively in or enriched in EEL-1 LD. The *dashed line* denotes the point of equivalency between GS::EEL-1 and GS::EEL-1 LD. *H*, summary of EEL-1 affinity purification proteomics data. OGT-1 is identified in GS::EEL-1 and GS::EEL- LD but absent in GS::GFP. OGT-1 was identified at similar levels in GS::EEL-1 and GS::EEL-1 LD when samples were normalized to the amount of EEL-1 target. For *C*, comparisons between genotypes represent pairwise two-way ANOVAs. Comparisons in the *inset* represent Fisher's LSD post hoc test. For *H*, significance was determined using Student's *t* test. ***, $p < 0.001$; *ns*, not significant ($p > 0.05$).

LD or GS::GFP (Fig. 2*C*). Previous work showed that locomotion, the behavioral output of the motor circuit, is also impaired in *eel-1* mutants (20). Consistent with this, *eel-1* (*bgg1*) null mutants had defective baseline locomotion while swimming in liquid. Locomotion defects were partially rescued by GS::EEL-1, but not GS::EEL-1 LD or GS::GFP (Fig. S3).

Taken together, these results support several conclusions. First, the *eel-1* protein null allele, *bgg1*, is hypersensitive to aldicarb and impairs locomotion in liquid. Second, the GS::EEL-1 affinity puri-

fication reagent is functional and rescues *eel-1 (bgg1)*. Finally, failure of GS::EEL-1 LD to rescue defects in *eel-1* (*bgg1*) mutants indicates that EEL-1 ubiquitin ligase activity is required for motor circuit function and locomotion.

C. elegans proteomics identifies OGT-1 as a putative EEL-1 binding protein

Our strategy for EEL-1 affinity purification proteomics is portrayed in Fig. 2*D*. Transgenic animals expressing GS::EEL-1, GS::EEL-1 LD, or GS::GFP (negative control) on an *eel-1 (bgg1)* protein null background were grown in large-scale liquid culture, harvested, and frozen in liquid nitrogen. Frozen animals were cryomilled in liquid nitrogen–cooled cylinders to obtain micron–scale grindates that facilitated rapid lysis and protein extraction. Whole worm lysates were applied to IgG-Dynabeads to affinity capture protein complexes containing GS-tagged target proteins. Sample quality was assessed and optimized using two parameters: 1) immunoblotting (1% of sample) to confirm GS-tagged target proteins were successfully purified (Fig. S4) and 2) silver staining (9% of sample) to evaluate sample purity and estimate the total amount of purified target (Fig. S4). Using this approach, affinity purification procedures were extensively optimized to obtain as much GS target as possible, while also ensuring that the GS::GFP negative control was as clean as possible compared with GS::EEL-1 and GS::EEL-1 LD test samples.

The majority of each sample (90%) was run on SDS-PAGE and subjected to in-gel trypsin digestion, and peptides were identified by LC-MS/MS (Fig. 2*D*). The most prominent species present in all samples were the affinity purification targets, GS::EEL-1, GS::EEL-1 LD, or GS::GFP (Fig. 2, *F* and *H*). Across four independent proteomic experiments, we identified 23 other proteins that were exclusive to, or enriched ≥2-fold in, the GS::EEL-1 or GS::EEL-1 LD samples compared with GS::GFP (Fig. 2*F* and Table S1). 13 proteins were either unique to WT GS::EEL-1 or present in both WT GS::EEL-1 and GS::EEL-1 LD samples (Fig. 2, *F* and *G*) and Table S1). These proteins represented putative EEL-1 binding proteins. 10 proteins were exclusive to or enriched in the GS::EEL-1 LD sample, which suggested that these proteins could be putative ubiquitination substrates (Fig. 2*G* and Table S1).

Two putative EEL-1 binding proteins were the most prominent: the glycosyltransferase OGT-1 (Fig. 2, *E–H*) and UBQ-1 (ubiquitin 1) (Fig. 2, *F–H*). It was not surprising that UBQ-1 co-purified with EEL-1 for two reasons: 1) HECT family E3 ubiquitin ligases, such as EEL-1, bind directly to ubiquitin and transfer it to substrates (38), and 2) EEL-1 contains a UBA-like domain, which binds polyubiquitin chains. Proteomics with *C. elegans* EEL-1 has not been performed before, and no EEL-1 binding proteins have previously been reported. Also, none of these putative EEL-1 binding proteins and putative EEL-1 ubiquitination targets have been described for the EEL-1 ortholog HUWE1 in prior studies (37–43).

In contrast to UBQ-1, the cytosolic and nuclear *O*-GlcNAc transferase OGT-1 was a novel, interesting putative EEL-1 binding protein (Fig. 2, *E–H*). OGT-1 spectra were found exclusively in GS::EEL-1 and GS::EEL-1 LD samples with sequence coverage of 27 and 41%, respectively (Fig. S5). To determine whether there was an increased number of OGT-1 peptides associated with EEL-1 LD compared with WT EEL-1, we normalized the total number of OGT-1 peptides to the total number of EEL-1 target peptides. Importantly, this was feasible because we performed four blinded, independent proteomic experiments. Normalization indicated that OGT-1 was present at similar levels and not significantly enriched in EEL-1 LD samples compared with WT EEL-1 samples (Fig. 2, *G* and *H*). These results suggest that OGT-1 is more likely to be an EEL-1 binding protein than an EEL-1 ubiquitination substrate, although they do not rule out the possibility that OGT-1 is ubiquitinated by EEL-1. Because OGT-1 potentially forms a complex with EEL-1, we prioritized investigating the biological relationship between these two proteins further.

OGT-1 is a conserved EEL-1 binding protein that forms a protein complex in neurons

To validate EEL-1 binding to OGT-1, we used co-immunoprecipitation (co-IP) from *C. elegans*. Transgenic worms were generated that express a fusion protein of GFP and EEL-1 (GFP::EEL-1) alone or in combination with FLAG epitope–tagged OGT-1 (FLAG::OGT-1). Transgenes were expressed using the *rgef-1* promoter, which drives expression in the worm nervous system. When FLAG::OGT-1 was precipitated from whole worm lysates, we observed robust coprecipitation of GFP::EEL-1 (Fig. 3*A*). Similarly, FLAG::OGT-1 coprecipitated with GFP::EEL-1 but not GFP alone when co-IP was performed in the opposite orientation (Fig. S6).

To determine whether OGT-1 is a conserved EEL-1 binding protein, we tested whether this interaction occurs between HUWE1 and OGT, the sole human orthologs of EEL-1 and OGT-1. We observed co-IP of FLAG-OGT with human GFP-HUWE1 from transfected HEK 293 cells (Fig. 3*B*). These results indicate that EEL-1 binds OGT-1 in neurons *in vivo* and that this interaction is conserved between human HUWE1 and OGT.

OGT-1 is expressed in the motor circuit and localizes to GABA presynaptic terminals

We previously showed that *eel-1* is expressed broadly in the nervous system, including both cholinergic and GABAergic motor neurons (20). Because proteomic and biochemical results indicate that EEL-1 and OGT-1 form a protein complex (Figs. 2 and 3), we wanted to evaluate *ogt-1* expression in the nervous system.

Previous work using an OGT-1 translational GFP reporter showed that OGT-1 is widely expressed in intestine, hypodermis, and neurons (44). To confirm this expression pattern and further characterize *ogt-1* neuronal expression, we generated transgenic animals that express an *ogt-1* transcriptional GFP reporter. We observed *ogt-1* expression broadly in the nervous system, as well as in pharyngeal muscle, intestine, and vulva (Fig. 4*A*). To determine whether *ogt-1* is expressed in the motor circuit, we coexpressed the *ogt-1* transcriptional GFP reporter with markers for either cholinergic ($P_{unc-129}$ mCherry) or GABAergic (P_{unc-25} mCherry) motor neurons. We observed coexpression of GFP with mCherry in both cholinergic (Fig. 4*B*) and GABAergic motor neurons (Fig. 4*C*). Thus, *ogt-1* is expressed in both

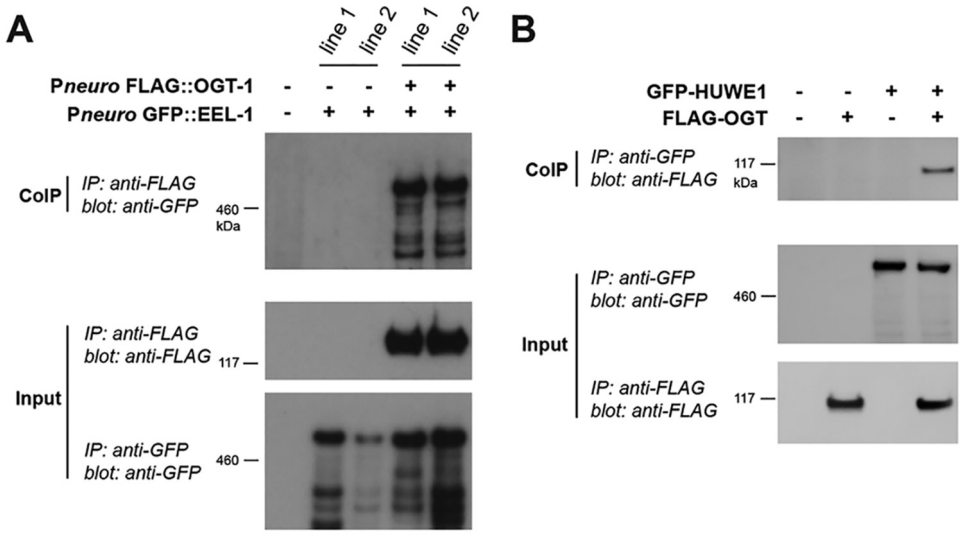

Figure 3. OGT-1 is a conserved EEL-1 binding protein that interacts with EEL-1 in neurons. *A*, GFP::EEL-1 was expressed alone or with FLAG::OGT-1 in the nervous system of *C. elegans*. Co-IP from transgenic worm lysates shows that GFP::EEL-1 binds FLAG::OGT-1. *B*, co-IP showing human GFP::HUWE1 binds to human FLAG::OGT when expressed in HEK 293 cells. Shown are representative images from three or more independent experiments.

cholinergic and GABAergic neurons of the *C. elegans* motor circuit, similar to *eel-1*.

We previously showed that EEL-1 is localized to presynaptic terminals in GABAergic motor neurons (20). Therefore, we evaluated where OGT-1 localizes in GABAergic motor neurons. To do so, we generated transgenic extrachromosomal arrays that use a GABA neuron promoter to express mCherry::OGT-1. This transgenic array was generated on a background that carried a second integrated transgene that expressed the synaptic vesicle marker SNB-1 (Synaptobrevin-1) fused to GFP (SNB-1::GFP) in GABA neurons. We found that mCherry::OGT-1 colocalized with SNB-1::GFP at presynaptic terminals of GABA motor neurons (Fig. 4*D*). This indicates that OGT-1 is present at presynaptic terminals in GABA neurons, similar to what was previously observed for EEL-1.

OGT-1 functions in GABA neurons to affect motor circuit function

Prior work using both electrophysiology and pharmacological approaches showed that EEL-1 regulates GABAergic presynaptic transmission, thereby impacting motor circuit function (20). Because OGT-1 binds EEL-1 (Figs. 2 and 3*A* and Fig. S6), is expressed in GABAergic motor neurons (Fig. 4*C*), and localizes to GABAergic presynaptic terminals like EEL-1 (Fig. 4*D*), we tested how OGT-1 affects motor circuit function using the automated aldicarb assay described earlier (Fig. 1). We evaluated two *ogt-1* mutants, *ok430* and *ok1474*. These are both large insertion/deletions that introduce premature stop codons upstream of the glycosyltransferase domain and are likely null alleles (45, 46). Both *ogt-1* (*ok430*) and *ogt-1* (*ok1474*) mutants were mildly hypersensitive to aldicarb (Fig. 5, *A* and *C* and Figs. S2*B* and S7). Aldicarb hypersensitivity was rescued by Mos1-mediated single-copy insertion (MosSCI) of OGT-1 using the pan-neuronal *rab-3* promoter (Fig. 5*A* and Figs. S2*B* and S7). Single-copy expression of OGT-1 in GABA neurons using the *unc-47* promoter also significantly rescued aldicarb hypersensitivity defects in *ogt-1 (ok430)* mutants (Fig. 5*A* and Fig. S2*B*). Weaker rescue with the GABA neuron promoter compared with the pan-neuronal driver might occur for two reasons. The GABA-specific promoter we used might not express OGT-1 at appropriate levels for rescue. Alternatively, OGT-1 could function in other types of neurons to contribute to aldicarb hypersensitivity. Nevertheless, these results show that OGT-1 functions in GABA neurons to regulate motor circuit function in *C. elegans*.

ogt-1 and eel-1 function in parallel to regulate motor circuit function and locomotion

We showed that OGT-1 functions in GABAergic motor neurons to regulate motor circuit function as assessed by aldicarb pharmacology (Fig. 5*A*). Because this result is similar to prior findings with EEL-1 (20), we investigated the genetic relationship between *ogt-1* (*ok430*) and *eel-1* (*bgg1*) mutants using automated aldicarb assays. Interestingly, *eel-1; ogt-1* double mutants showed enhanced aldicarb hypersensitivity compared with *eel-1* single mutants at low aldicarb dose (8 μM) (Fig. 5*B*). Enhanced hypersensitivity was observed across aldicarb dose response for *eel-1; ogt-1* double mutants compared with *eel-1* mutants (Fig. 5*C*). To ensure that enhanced aldicarb hypersensitivity was not due to effects on locomotion, speed was normalized to no drug controls for each genotype for these experiments. Enhanced hypersensitivity to aldicarb displayed by *eel-1; ogt-1* double mutants was rescued by using MosSCI to express OGT-1 in the nervous system (Fig. 5*D*). These results indicate that *eel-1* and *ogt-1* function in parallel in neurons to affect aldicarb sensitivity.

To further assess how genetic interactions between *ogt-1* and *eel-1* influence motor circuit function, we analyzed locomotion using MWT to monitor swimming speed. *ogt-1* mutants had a mild defect in swim speed compared with WT animals, and *eel-1* mutants were moderately impaired (Fig. 5*E*). Importantly,

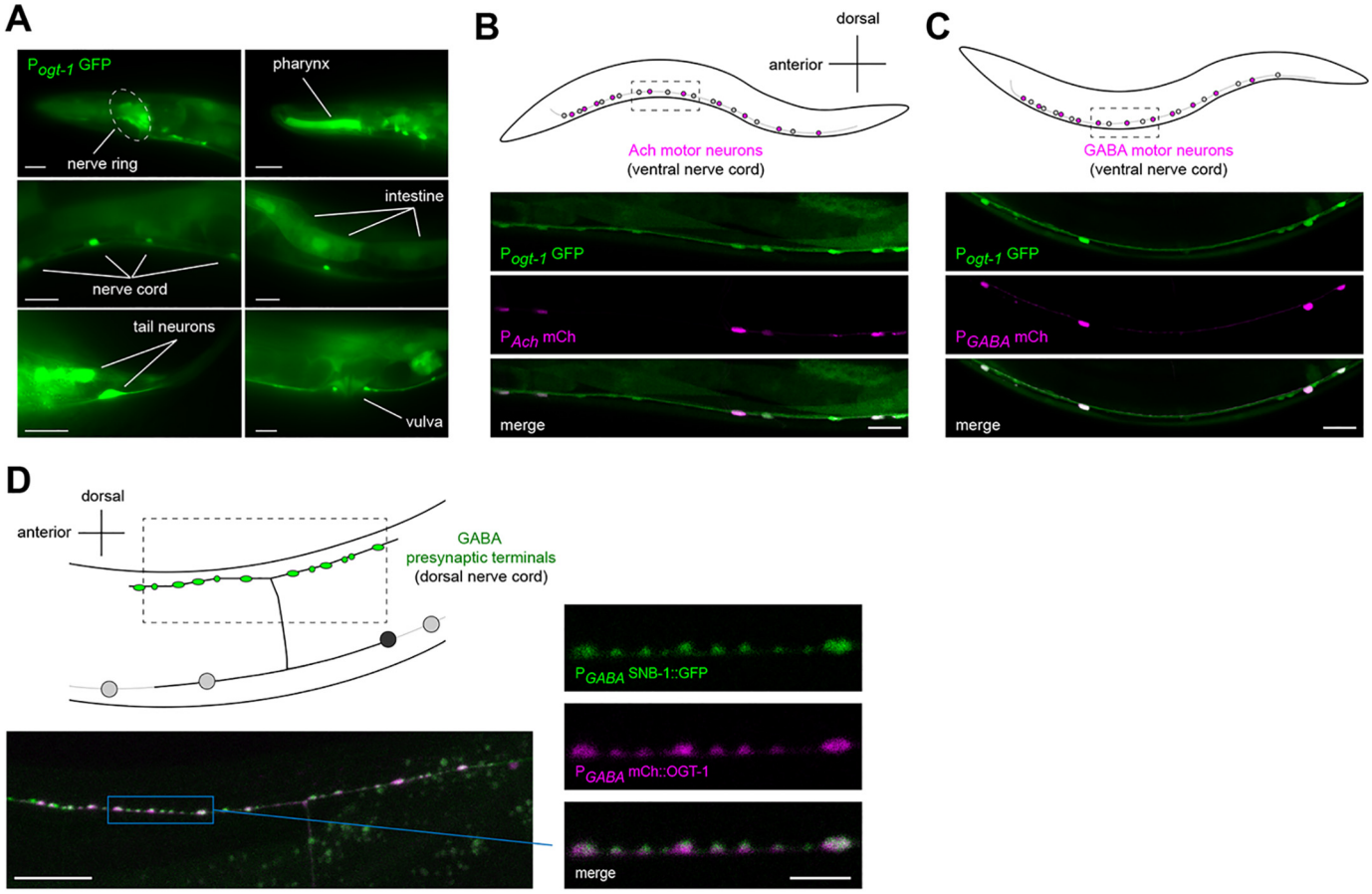

Figure 4. OGT-1 is expressed in cholinergic and GABAergic motor neurons and localizes to GABAergic presynaptic terminals. *A*, representative epifluorescent images showing that GFP driven by the *ogt-1* promoter (P_{ogt-1} GFP) is broadly expressed inside and outside the nervous system. *B* and *C*, schematic and representative confocal images showing that GFP expressed using the *ogt-1* promoter (P_{ogt-1} GFP) coexpresses with markers for cholinergic (*B*) and GABAergic (*C*) motor neurons. *D*, schematic and representative confocal images showing that mCherry::OGT-1 colocalizes with synaptic vesicle marker SNB-1::GFP at presynaptic terminals of GABAergic motor neurons. Shown are maximum intensity *z*-projection (*left*) and single *z*-slices (*right*) from the indicated region (*blue box*). All *scale bars* are 20 μm except for the one in the *right panel* of *D*, which is 5 μm.

eel-1; ogt-1 double mutants showed enhanced decreases in swim speed compared with *eel-1* single mutants (Fig. 5*E*). Genetic enhancer effects between *ogt-1* and *eel-1* were also observed when brood size and viability were evaluated (Fig. S8). Thus, OGT-1 and EEL-1 function in parallel to affect multiple phenotypes with prominent effects on motor circuit function and locomotion.

OGT-1 does not affect synapse formation in GABA motor neurons

Next, we evaluated a straightforward hypothesis that might explain how OGT-1 and EEL-1 function in parallel to regulate GABA neuron function: Do OGT-1 and EEL-1 function in parallel to affect synapse formation in GABA neurons? To test this, we analyzed the distribution and pairing of pre- and postsynaptic markers at GABAergic neuromuscular junctions (NMJs). As a presynaptic marker, we used an integrated transgenic array that expresses SNB-1::GFP in GABA motor neurons (Fig. 6*A*). To postsynaptically label GABA synapses, we used a single-copy transgene that expresses the GABA receptor subunit UNC-49 fused to TagRFP (UNC-49::RFP) (Fig. 6*A*). Results from confocal microscopy indicated that pairing of pre- and postsynaptic terminals was normal in *ogt-1* (*ok430*) mutants and *eel-1* (*bgg1*) mutants (Fig. 6*B*). Similarly, pre- and postsynaptic pairing was normal in *eel-1; ogt-1* double mutants (Fig. 6*B*). Quantitation of the number of SNB-1::GFP puncta showed no defects in single mutants or *eel-1; ogt-1* double mutants (Fig. 6*C*). These results demonstrate that synapse formation is not impaired at GABAergic NMJs of *eel-1; ogt-1* double mutants and rules this out as an explanation for enhanced defects in aldicarb hypersensitivity and locomotion in these double mutants.

OGT-1 glycosyltransferase activity is dispensable for motor circuit function

To begin deciphering how OGT-1 affects motor circuit function, we tested whether OGT-1 glycosyltransferase activity is involved. To do so, we evaluated whether point mutations in OGT-1 that impair glycosyltransferase activity can rescue aldicarb hypersensitivity of *ogt-1* null mutants. We tested two point mutants, OGT-1 *K957M* and *H612A*, that affect conserved residues known to completely abolish and strongly impair glycosyltransferase activity of OGT-1 orthologs, respectively (47–49). Interestingly, we observed similar strong rescue when MosSCI was used to pan-neuronally express WT OGT-1, OGT-1 *K957M*, or OGT-1 *H612A* (Fig. 7, *A* and *B*). These results demonstrate that OGT-1 functions independent of

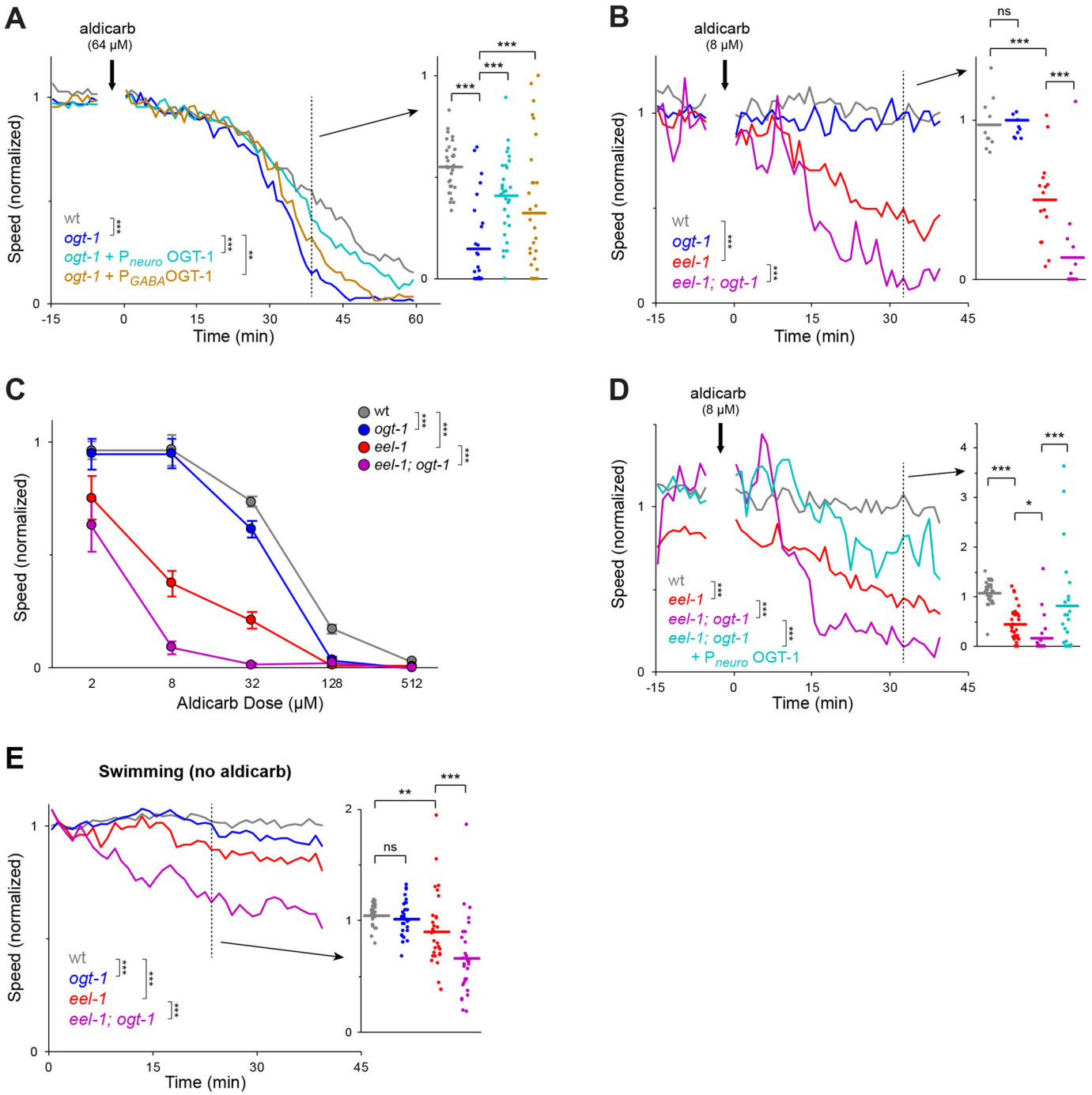

Figure 5. *ogt-1* functions in GABA neurons to regulate aldicarb sensitivity and enhances *eel-1*. Shown are automated aldicarb assays with speed normalized to the buffer-only control group for each genotype. *A*, *ogt-1* (*ok430*) mutants are hypersensitive to a moderate aldicarb dose (64 μM) compared with WT. Aldicarb hypersensitivity is rescued by transgenic expression of OGT-1 pan-neuronally or in GABA neurons. Shown are means of multiple wells for each genotype ($n = 29–30$ wells, 4 worms/well). *Inset*, mean speed (*line*) and individual data points at the indicated time. *B*, *eel-1* (*bgg1*) mutants are hypersensitive to low aldicarb dose (8 μM) compared with WT, and hypersensitivity is enhanced in *ogt-1; eel-1* double mutants. Shown are means ($n = 10–15$ wells). *C*, dose response showing that *ogt-1* mutants are hypersensitive to moderate and high doses of aldicarb. Aldicarb hypersensitivity is enhanced in *ogt-1; eel-1* double mutants across doses. Shown are mean ± S.E. for normalized speed 35 min after aldicarb exposure ($n = 5–15$ wells). *D*, OGT-1 expressed in neurons rescues enhanced aldicarb hypersensitivity of *ogt-1; eel-1* double mutants. Shown are means ($n = 30$ wells for each genotype, 1 worm/well due to *ogt-1; eel-1* low brood size). *E*, automated analysis of swimming speed for indicated genotypes. Swimming defects in *eel-1* and *ogt-1* single mutants are enhanced in *ogt-1; eel-1* double mutants ($n = 30–65$ wells). *Inset*, mean speed (*line*) and individual data points at the indicated time. Comparisons between genotypes represent pairwise two-way ANOVAs. Comparisons in the *inset* represent Fisher's LSD post hoc test (see Fig. S2*B* for further statistical analysis). **, $p < 0.01$; ***, $p < 0.001$; *ns*, not significant ($p > 0.05$).

enzymatic glycosyltransferase activity to regulate motor circuit function.

As an independent approach to address this question, we asked whether loss of OGA-1 (*O*-GlcNAcase 1), which has opposing enzymatic activity to OGT-1 (46), affects motor circuit function. If motor circuit function is affected by *O*-GlcNAcylation, *oga-1* mutants would be expected to have the opposite phenotype to *ogt-1* mutants. In the case of auto-

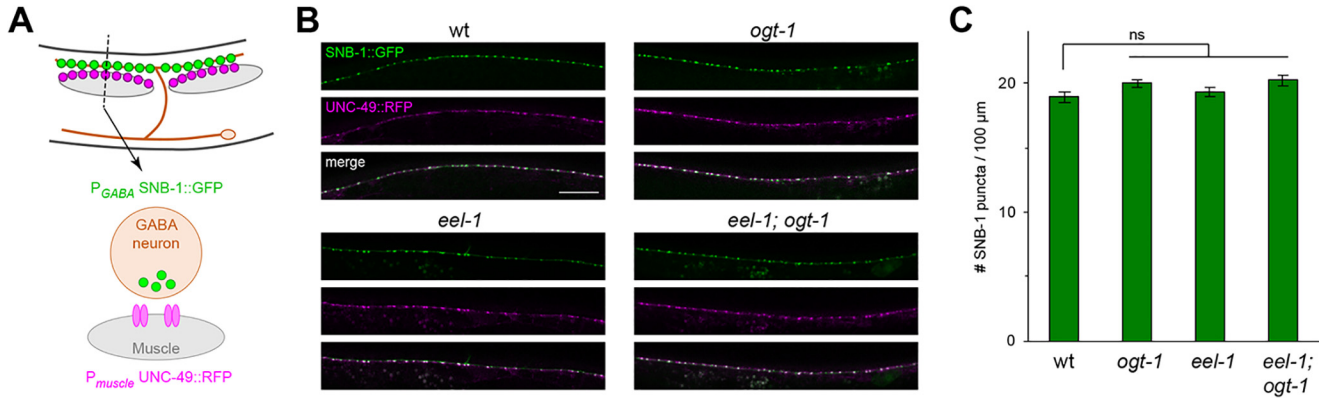

Figure 6. GABA synapse formation is not impaired in *eel-1; ogt-1* double mutants. *A*, schematic of GABA NMJs in *C. elegans* dorsal cord. SNB-1::GFP marks GABA presynaptic terminals and GABA receptor subunit, and UNC-49::RFP marks postsynaptic terminals. *B*, representative confocal images showing colocalization of presynaptic SNB-1::GFP and postsynaptic UNC-49::RFP is normal for all indicated genotypes. *C*, quantitation indicates that the number of SNB-1::GFP puncta is not changed for any genotype. Shown are mean ± S.E. (*error bars*) ($n = 38–44$ worms). Significance was tested using ANOVA. *ns*, not significant ($p > 0.05$). *Scale bar*, 20 μM.

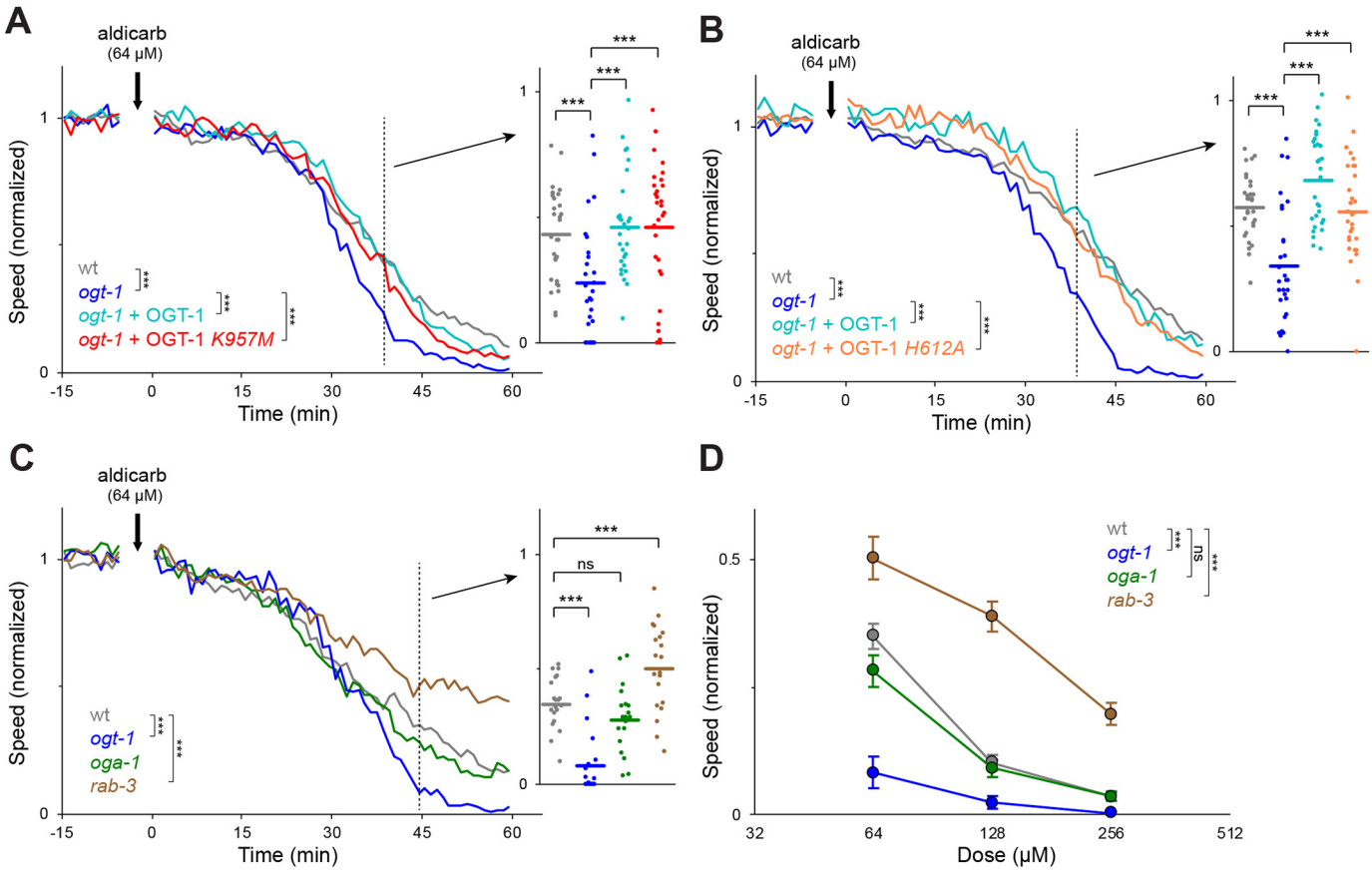

Figure 7. OGT-1 glycosyltransferase activity is not required for motor circuit function. Shown are automated aldicarb assays with speed normalized to buffer-only control group for each genotype. Aldicarb hypersensitivity in *ogt-1* (*ok430*) mutants is significantly rescued by pan-neuronal expression of two OGT-1 point mutants that lack catalytic glycosyltransferase activity: OGT-1 *K957M* (*A*) and OGT-1 *H612A* (*B*) ($n = 30$ wells, 4 worms/well). *C*, *oga-1* (*ok1207*) mutants have similar aldicarb hypersensitivity as WT animals. Note that *ogt-1* (*ok430*) and *rab-3* (*js49*) mutants are included as controls for aldicarb hypersensitivity and resistance, respectively. *D*, dose response showing that *oga-1* mutants have similar responses to aldicarb as WT animals. Shown are mean ± S.E. (*error bars*) for normalized speed 45 min after aldicarb exposure ($n = 20$ wells). Comparisons between genotypes represent pairwise two-way ANOVAs. Comparisons in the *inset* represent Fisher's LSD post hoc tests. ***, $p < 0.001$; *ns*, not significant ($p > 0.05$).

mated aldicarb assays, this would be resistance to aldicarb paralysis rather than hypersensitivity displayed by *ogt-1* mutants (Fig. 5, *A* and *C*). To ensure that our automated aldicarb assay can accurately evaluate aldicarb resistance, we tested *rab-3* mutants, which are mildly resistant to aldicarb (34). Indeed, *rab-3* mutants were resistant to aldicarb compared with WT animals in our automated liquid assay (Fig. 7, *C* and *D*). In contrast, *oga-1* null mutants had similar aldicarb sensitivity to WT animals across a range of doses (Fig. 7, *C* and *D*). Taken together, these results with catalytically inactive OGT-1 point mutants and *oga-1* mutants suggest that OGT-1 does not rely upon glycosyltransferase activity to affect motor circuit function.

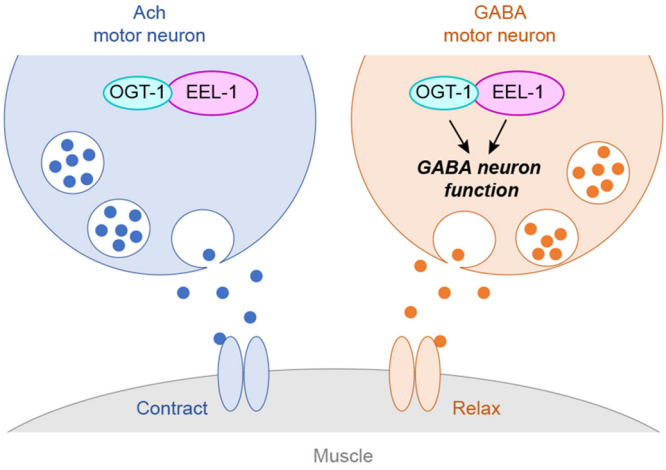

Figure 8. OGT-1 and EEL-1 form a protein complex and regulate GABA neuron function in *C. elegans* motor circuit. Shown is a summary of our findings that OGT-1 and EEL-1 form a complex *in vivo* in *C. elegans* neurons. OGT-1 and EEL-1 are expressed in both cholinergic and GABAergic motor neurons but function in parallel to regulate GABA neuron function.

Discussion

OGT-1 forms a protein complex with EEL-1 and affects GABA neuron function

We previously showed that the EEL-1 E3 ubiquitin ligase, a gigantic protein broadly expressed in the nervous system, plays an important role in motor circuit function by regulating presynaptic GABAergic transmission (20). We now provide evidence that EEL-1 ubiquitin ligase activity affects aldicarb sensitivity and locomotion, and therefore is likely to be involved in this process (Fig. 2*C* and Fig. S3).

To begin further deciphering how EEL-1 regulates GABAergic transmission, we used affinity purification proteomics from *C. elegans* to identify EEL-1 binding proteins. This approach identified the OGT-1 *O*-GlcNAc transferase as a prominent EEL-1 binding protein (Fig. 2, *E–H*). Biochemical results from *C. elegans* indicate that OGT-1 binds EEL-1 in neurons *in vivo* (Fig. 3*A* and Fig. S6). Like EEL-1, OGT-1 is expressed broadly in the nervous system, including the motor circuit, and localizes to GABAergic presynaptic terminals (Fig. 4). Results from an automated pharmacological assay showed that OGT-1 functions in GABAergic motor neurons to affect motor circuit function (Fig. 5*A* and Fig. S2*B*). Interestingly, our genetic results show that defects in motor circuit function are enhanced in *ogt-1; eel-1* double mutants (Fig. 5, *B–D*). Consistent with this, enhanced defects in locomotion were also observed in *eel-1; ogt-1* double mutants (Fig. 5*E*). Taken together, our results and prior findings support the conclusion that OGT-1 and EEL-1 form a complex and function in parallel to affect GABA neuron function, thereby influencing the motor circuit and locomotion (Fig. 8). In the future, more extensive physiological and cellular studies will be useful to further test this model. Nonetheless, it is noteworthy that our findings are the first example of OGT-1 or its orthologs forming a complex with a ubiquitin ligase to affect a common process in any system.

Two observations suggest that OGT-1 may not be ubiquitinated by EEL-1. First, EEL-1 affinity purification proteomics was done with two EEL-1 constructs, WT EEL-1 and EEL-1 LD (Fig. 2). Because EEL-1 LD cannot ubiquitinate targets, it potentially enriches ubiquitination substrates. Consistent with this, we detected several proteins that were exclusive to or enriched in EEL-1 LD samples, which represent putative ubiquitination substrates (Fig. 2*G* and Table S1). In contrast, OGT-1 was not significantly enriched in normalized EEL-1 LD samples (Fig. 2, *G* and *H*). The second argument is based on genetics. We observed that aldicarb hypersensitivity was enhanced in *ogt-1; eel-1* double mutants (Fig. 5, *B–D*), which indicates that *ogt-1* and *eel-1* function in parallel to regulate GABA neuron function. If EEL-1 ubiquitinates OGT-1, we would expect a genetic relationship reflective of same pathway genetics, such as suppression or no increased effects in double mutants, neither of which occurred. Thus, our findings with affinity purification proteomics and loss-of-function genetics do not rule out the possibility that OGT-1 is ubiquitinated by EEL-1 but do suggest that this is unlikely in the context of GABA neuron function.

At present, the function of *C. elegans* OGT-1 and mammalian OGT in the nervous system remains minimally explored. Our results show that OGT-1 is expressed broadly throughout the nervous system, including both excitatory cholinergic and inhibitory GABAergic neurons in the motor circuit (Fig. 4, *A–C*). This suggests that OGT-1 could have wide-ranging functions in the nervous system and could affect both excitatory and inhibitory motor neuron function. However, *ogt-1* mutants are hypersensitive to aldicarb, and hypersensitivity is rescued by OGT-1 expression in GABA neurons (Fig. 5*A* and Fig. S2*B*). Furthermore, aldicarb hypersensitivity in *ogt-1* mutants is enhanced by *eel-1*, a known regulator of presynaptic GABAergic transmission (20). This suggests that the OGT-1/EEL-1 complex is likely to preferentially affect GABA neuron function. Consistent with this, a prior study in mammals showed that OGT regulates the activity of GABAergic AgRP neurons (32). Moving forward, it will be important to address whether the OGT-1/EEL-1 complex is a conserved regulator of GABA neuron function and determine how this complex regulates GABA neuron function.

As an initial foray into addressing this question, we show that OGT-1 does not require enzymatic glycosyltransferase activity to regulate motor circuit function. This is supported by results using two different conserved mutations that impair OGT-1 glycosyltransferase activity, one of which completely abolishes enzymatic activity (Fig. 7, *A* and *B*). Consistent with this, motor circuit function was not affected by OGA-1, which removes *O*-GlcNAc and opposes the activity of OGT-1 (Fig. 7, *C* and *D*). While prior studies have shown that OGT-1 has nonenzymatic activities, such as acting as a scaffold protein, these remain understudied (25). Importantly, it is unknown whether OGT has nonenzymatic functions in the nervous system. Our results using an *in vivo* model system now suggest that OGT-1 functions independent of glycosyltransferase activity and in a complex with EEL-1 to regulate GABA neuron function.

Interestingly, many of our observations on the OGT-1/EEL-1 complex share similarities with prior findings on the OGT/mSin3A complex that represses transcription (50). In both cases, OGT glycosyltransferase activity is dispensable, and OGT acts in parallel to the enzymatic activity of its binding

partner. Thus, our work and this prior study highlight core biochemical principles at play in OGT complexes that act independently of glycosyltransferase activity.

Implications of the OGT/HUWE1 complex in cell biology and disease

Our discovery of the OGT-1/EEL-1 complex could have broad implications within the nervous system, outside the nervous system, and across species. We found that the physical interaction between OGT-1 and EEL-1 is conserved between the human orthologs, OGT and HUWE1 (Fig. 3*B*). Thus, the interaction between OGT and HUWE1 is conserved in human cells and could be functionally relevant across species. Consistent with our findings, two prior affinity purification proteomic studies with HEK 293 cells hinted at the possibility of an OGT/HUWE1 complex (51, 52). We now show that an OGT/HUWE1 complex exists, the interaction between OGT and HUWE1 is evolutionarily conserved, and these molecules have functional genetic interactions in *C. elegans* that affect GABA neuron function and locomotion.

Consistent with our results, previous studies that examined OGT or HUWE1 independently indicate that these molecules converge on several cellular functions as well as during disease. Both OGT and HUWE1 (also called Arf-BP1/Mule) are implicated in oncogenesis and regulate the transcription factor Myc (53, 54). In the nervous system, both HUWE1 and OGT affect neural progenitor proliferation (37, 40, 55, 56) and mitochondrial function (30, 57–59). Moreover, genetic changes in both *HUWE1* and *OGT* are linked to intellectual disability. Human genetic studies have shown that both increases in copy number and missense mutations in *HUWE1* result in intellectual disability (21–23). Because some disorder-associated point mutations in *HUWE1* are loss-of-function, it is likely that both increased and reduced HUWE1 function are associated with intellectual disability (20). In recent human genetic studies, three different mutations in *OGT* were suggested to cause intellectual disability (60, 61). Thus, our discovery of a conserved, functionally relevant OGT-1/EEL-1 complex not only informs our understanding of how GABA neuron function is regulated in a model circuit, but could have important implications for oncogenesis, neural progenitor proliferation, mitochondrial function, and intellectual disability.

Experimental procedures

C. elegans genetics and transgenics

C. elegans were maintained using standard protocols (62) and were cultivated at 23 °C for experiments unless noted otherwise. WT strain was N2 isolate. Mutant alleles included *goa-1* (*n363*), *slo-1* (*js379*), *unc-25* (*e156*), *unc-49* (*e407*), *unc-119* (*ed3*), *pha-1* (*e2123*), *eel-1* (*zu462*), *eel-1* (*bgg1*), *ogt-1* (*ok430*), *ogt-1* (*ok1474*), *oga-1* (*ok1207*), *rab-3* (*js49*). Transgenic alleles included *ttTi16881* [Mos1], *ttTi5605* [Mos1], *bggIs16* [P_{eel-1} EEL-1], *bggIs31* [P_{eel-1} GS::EEL-1], *bggIs32* [P_{eel-1} GS::GFP], *bggIs33* [P_{eel-1} GS::EEL-1(*C4144A*)], *bggSi2* [P_{rab-3} OGT-1], *bggSi19* [P_{unc-47} OGT-1], *bggSi21* [P_{rab-3} OGT-1 *H612A*], *bggSi22* [P_{rab-3} OGT-1 *K957M*], *juIs1* [P_{unc-25} SNB-1::GFP], *krSi2* [P_{unc-49} UNC-49B::TagRFP]. For experiments with *eel-1; ogt-1* double mutants, *eel-1* was balanced using *tmC25* [*tmIs1241*] to maintain the strain because of defects in brood size and viability (Fig. S8). As controls, WT animals and single mutants were also balanced. Homozygous unbalanced strains were selected for at least two generations before testing to avoid maternal effects.

Construction details for transgenic alleles are described in Table S2 and were made using standard procedures (63, 64). Plasmid details and sequences are available upon request.

Automated assays for aldicarb and swim speed

Synchronized young adults (20 h after L4) were loaded into 20 wells (4 animals/well) with 20 μl of assay buffer (0.01% Tween 20 in M9). Baseline behavior was recorded for 10 min, 10 μl of aldicarb was added at the desired concentration, and recording continued. Behavioral recordings were taken using MWT (65) with a Toshiba-Teli Ultra high-resolution 12 megapixel CMOS sensor camera-link camera (CSC12M25BMP19-01B) and Qioptiq Rodagon-F 50-mm f/2.8 lens (0703-089-000-24).

Custom-written scripts calculated the mean speed every minute per well. For Figs. 1 and 2, speed was normalized to baseline (10 min of swimming in the absence of aldicarb) for each genotype. For Fig. 5, speed was normalized to no aldicarb controls for the length of the experiment to rule out effects of a given genotype on locomotion. This was particularly important for *eel-1; ogt-1* double mutants that displayed enhanced defects in both aldicarb paralysis (Fig. 5, *B–D*) and swimming speed in the absence of aldicarb (Fig. 5*E*). Note paralysis threshold was defined as at or below 0.02 mm/s. For locomotion analysis in Fig. 5*E*, speed across all time points was normalized to the first 5 min of the assay for each genotype.

C. elegans affinity purification proteomics

Animals were liquid-cultured for 4 days (66), harvested by centrifugation, separated on 30% sucrose flotation, and washed three times. Packed worms were resuspended in an equal volume of 50 mM NaCl and frozen as pellets in liquid N_2. Pellets were cryomilled (Retsch) with protease inhibitors (Complete, Roche Applied Science) and lysed in 3× volume lysis buffer (50 mM Tris-HCl (pH 7.5), 150 mM NaCl, 1.5 mM $MgCl_2$, 10% glycerol, 0.1% Nonidet P-40, 1 mM DTT, 1 mM phenylmethylsulfonyl fluoride, 1.5× Halt Protease Inhibitor Mixture (Thermo Scientific), 1 mM sodium orthovanadate, 5 mM sodium fluoride, 1 mM sodium molybdate). Lysate was rotated for 10 min at 4 °C and centrifuged at 20,000 × *g* for 10 min.

Volume of lysate required for 200 mg of total protein was incubated with 400 μl of IgG-coated Dynabeads (Invitrogen) for 1 h at 4 °C. Following affinity capture, beads were washed five times with lysis buffer. Purification quality was assessed by immunoblotting 1% of sample (anti-SBP antibody, Sigma-Aldrich) and silver staining 9% of the sample (Thermo Scientific). The remaining 90% of the sample was run on SDS-PAGE, subject to in-gel trypsin digestion, and run on LC-MS/MS. Prior to MS analysis, pooled peptides were acidified, desalted with a Zip-Tip C18 column, dried, and resuspended in 100 μl of 0.1% formic acid. 13 μl of sample was used per MS run. Samples were analyzed using an Orbitrap Fusion™ Tribrid™ mass spectrometer (Thermo Fisher Scientific) coupled to an EASY-nLC 1000 system. Peptides were eluted on an analytical RP column (0.075 × 250-mm Acclaim PepMap RLSC nano Viper, Thermo

Fisher Scientific), operating at 300 nl/min using the following gradient: 5–25% B for 40 min, 25–44% B for 20 min, 44–80% B in 10 s, 80% B for 5 min, 80–5% in 10 s, and 5% B for 20 min (solvent A: 0.1% formic acid (v/v); solvent B: 0.1% formic acid (v/v), 80% CH3CN (v/v) (Fisher)). The Orbitrap Fusion was operated in a data-dependent MS/MS mode using the 10 most intense precursors detected in a survey scan from 380 to 1,400 m/z performed at 120,000 resolution. Tandem MS was performed by HCD fragmentation with normalized collision energy of 30.0%.

Spectra were analyzed using Mascot (Matrix Science) and Sequest (Thermo Fisher Scientific). Mascot and Sequest were set up to search the *C. elegans* proteome (UniProt, May 2017, 27,483 entries). Analysis parameters included fragment ion mass tolerance of 20 ppm (Mascot) or 0.02 Da (Sequest) and parent ion tolerance of 10.0 ppm. Carbamidomethyl of cysteine was specified as a fixed modification, and deamidation of asparagine and glutamine and oxidation of methionine were specified as variable modifications.

Scaffold (Proteome Software) was used to validate MS/MS-based peptide and protein identifications. Peptide identifications were accepted if they could be established at >5.0% probability to achieve a false discovery rate (FDR) < 1.0% by the Scaffold Local FDR algorithm. Protein identifications were accepted if they could be established at >98.0% probability to achieve an FDR <1.0% and contained at least two identified peptides. Protein probabilities were assigned by the Protein Prophet algorithm (67). EEL-1 binding proteins were identified using the following criteria: 1) the protein was detected in at least two of the four experiments; 2) the protein had 2× or more total spectra in the GS::EEL-1 or GS::EEL-1 LD samples compared with GS::GFP negative control; 3) ribosomal proteins were removed. Spectra were normalized by subtracting spectra from negative control (GS::GFP) and dividing by the target (EEL-1).

Biochemistry

For *C. elegans* biochemistry, animals were grown, processed, cryomilled, and lysed as discussed for proteomics. For biochemistry with HEK 293-T cells, cells were transfected with FLAG-OGT (pBG-GY845, 3 μg) and/or GFP-HUWE1 (pBG-GY896, 14 μg) using Lipofectamine 3000 (Invitrogen). OGT cDNA (NP_858059.1) was purchased (MGC, Dharmcon). HUWE1 cDNA was purchased (Addgene, catalog no. 37431), and two mutations were repaired to match HUWE1 (NP_113584.3). Cells were transfected initially with FLAG-OGT and 12 h later with GFP-HUWE1. 24 h after transfection, cells were lysed in buffer (50 mM Tris-HCl (pH 7.5), 150 mM NaCl, 10% glycerol, 0.1% Nonidet P-40, 1 mM DTT, and 1× HALT protease inhibitor mixture).

Lysates (10 mg of total protein *C. elegans*, 0.65 mg of total protein 293 cells) were incubated with primary antibody for 30 min and precipitated for 1 h (*C. elegans*) or 4 h (293 cells) with 10 μl of protein G–agarose (Roche Applied Science) at 4 °C. Antibodies used for IP included mouse monoclonal anti-FLAG (M2, Sigma-Aldrich) and anti-GFP (3E6, Invitrogen). Precipitates were boiled in sample buffer and run on 3–8% Tris acetate gels (Invitrogen). Gels were transferred overnight to polyvinylidene difluoride membranes and immunoblotted with either rabbit polyclonal anti-FLAG (Cell Signaling) or mouse monoclonal anti-GFP (Roche Applied Science) antibodies. Proteins were visualized using horseradish peroxidase–conjugated secondary antibodies (GE Healthcare Life Sciences, Fisher Scientific) and ECL (Supersignal West Femto or Pico, Thermo Scientific). Blots were imaged with X-ray film for *C. elegans* experiments and digitally imaged for 293 experiments (KwikQuant™ Imager).

Microscopy

Epifluorescence microscopy was performed using a Leica CFR5000 with a ×40 magnification oil-immersion lens. Images were acquired using a CCD camera (Leica DFC345 FX). Confocal microscopy was performed using a Leica TCS SP8 MP confocal microscope system with a ×25 or ×40 water immersion lens. Settings that avoided bleed-through between different channels were confirmed when collecting coexpression and colocalization. For colocalization experiments, images were acquired in resonant mode.

Young adult animals were anesthetized and mounted on 2% agar for imaging. When colocalization was being evaluated, animals were anesthetized with 5 mM levamisole in M9 buffer. Epifluorescent microscopy was used to quantitate SNB-1::GFP puncta with animals anesthetized using 1% 1-phenoxy-2-propanol in M9 buffer.

Brood size and viability assay

Individual L4 larvae were placed on fresh plates every 12 h for 4 days at 20 °C. Brood size was total eggs laid per animal over 4 days. Eggs were cultivated at ~23 °C for 3 days, and viability was measured as the percentage of eggs that developed to L4 stage or older.

Statistical analysis

For aldicarb and swim speed experiments, data were derived from multiple wells acquired across multiple independent experiments. Comparisons were made using two-way ANOVAs. If a significant effect or interaction was observed ($p < 0.05$), Fisher's LSD post hoc tests were performed to evaluate differences. Individual time points that best represented differences between genotypes were chosen for presentation as *insets*, but post hoc comparisons at all time points were also done (*e.g.* see Fig. S2). For proteomics, comparisons were made using Student's t test. For quantitation of SNB-1::GFP puncta, images were collected for each genotype from three independent experiments, and significance was tested using ANOVA. For brood size and viability, significance was assessed using ANOVA and Fisher's LSD post hoc tests.

Author contributions—A. C. G. designed, performed, and analyzed experiments using *C. elegans*. M. D. performed HEK 293 experiments. K. J. O. designed and generated *eel-1* (*bgg1*), constructed plasmids, isolated transgenic strains, and advised on design and implementation of affinity purification proteomics. R. T. constructed plasmids and isolated mutant and transgenic strains. M. J. M. constructed plasmids. B. G. provided supervision, aided in experimental design, and oversaw project design and implementation. A. C. G. and B. G. wrote and edited the manuscript.

Acknowledgments—We thank the Caenorhabditis Genetics Center for several alleles. We thank the Ewbank and Segalat laboratories (NEMAGENETAG project) and CNRS (UMS3421) for generation and distribution of ttTi16881. krSi2 was a kind gift of Dr. Jean-Louis Bessereau. tmC25 [tmIs1241] was provided by Dr. Shohei Mitani (National Bio-Resource Project, MEXT, Japan). We thank Rayna Birnbaum for technical assistance.

References

1. Huang, Z. J., and Scheiffele, P. (2008) GABA and neuroligin signaling: linking synaptic activity and adhesion in inhibitory synapse development. *Curr. Opin. Neurobiol.* **18,** 77–83 CrossRef Medline
2. Krueger-Burg, D., Papadopoulos, T., and Brose, N. (2017) Organizers of inhibitory synapses come of age. *Curr. Opin. Neurobiol.* **45,** 66–77 CrossRef Medline
3. Schuske, K., Beg, A. A., and Jorgensen, E. M. (2004) The GABA nervous system in *C. elegans*. *Trends Neurosci.* **27,** 407–414 CrossRef Medline
4. Zhen, M., and Samuel, A. D. (2015) C. elegans locomotion: small circuits, complex functions. *Curr. Opin. Neurobiol.* **33,** 117–126 CrossRef Medline
5. Ramamoorthi, K., and Lin, Y. (2011) The contribution of GABAergic dysfunction to neurodevelopmental disorders. *Trends Mol. Med.* **17,** 452–462 CrossRef Medline
6. Ko, J., Choii, G., and Um, J. W. (2015) The balancing act of GABAergic synapse organizers. *Trends Mol Med* **21,** 256–268 CrossRef Medline
7. Chapman, E. R. (2008) How does synaptotagmin trigger neurotransmitter release? *Annu. Rev. Biochem.* **77,** 615–641 CrossRef Medline
8. Südhof, T. C. (2012) The presynaptic active zone. *Neuron* **75,** 11–25 CrossRef Medline
9. Tretter, V., Jacob, T. C., Mukherjee, J., Fritschy, J. M., Pangalos, M. N., and Moss, S. J. (2008) The clustering of GABA(A) receptor subtypes at inhibitory synapses is facilitated via the direct binding of receptor α2 subunits to gephyrin. *J. Neurosci.* **28,** 1356–1365 CrossRef Medline
10. Poulopoulos, A., Aramuni, G., Meyer, G., Soykan, T., Hoon, M., Papadopoulos, T., Zhang, M., Paarmann, I., Fuchs, C., Harvey, K., Jedlicka, P., Schwarzacher, S. W., Betz, H., Harvey, R. J., Brose, N., *et al.* (2009) Neuroligin 2 drives postsynaptic assembly at perisomatic inhibitory synapses through gephyrin and collybistin. *Neuron* **63,** 628–642 CrossRef Medline
11. Takahashi, H., Katayama, K., Sohya, K., Miyamoto, H., Prasad, T., Matsumoto, Y., Ota, M., Yasuda, H., Tsumoto, T., Aruga, J., and Craig, A. M. (2012) Selective control of inhibitory synapse development by Slitrk3-PTPδ trans-synaptic interaction. *Nat. Neurosci.* **15,** 389–398, S1–S2 CrossRef Medline
12. Li, J., Han, W., Pelkey, K. A., Duan, J., Mao, X., Wang, Y. X., Craig, M. T., Dong, L., Petralia, R. S., McBain, C. J., and Lu, W. (2017) Molecular dissection of Neuroligin 2 and Slitrk3 reveals an essential framework for GABAergic synapse development. *Neuron* **96,** 808–826.e8 CrossRef Medline
13. Yamasaki, T., Hoyos-Ramirez, E., Martenson, J. S., Morimoto-Tomita, M., and Tomita, S. (2017) GARLH family proteins stabilize $GABA_A$ receptors at synapses. *Neuron* **93,** 1138–1152.e6 CrossRef Medline
14. Feng, J., Chi, P., Blanpied, T. A., Xu, Y., Magarinos, A. M., Ferreira, A., Takahashi, R. H., Kao, H. T., McEwen, B. S., Ryan, T. A., Augustine, G. J., and Greengard, P. (2002) Regulation of neurotransmitter release by synapsin III. *J. Neurosci.* **22,** 4372–4380 CrossRef Medline
15. Gitler, D., Takagishi, Y., Feng, J., Ren, Y., Rodriguiz, R. M., Wetsel, W. C., Greengard, P., and Augustine, G. J. (2004) Different presynaptic roles of synapsins at excitatory and inhibitory synapses. *J. Neurosci.* **24,** 11368–11380 CrossRef Medline
16. Barclay, J. W., Morgan, A., and Burgoyne, R. D. (2012) Neurotransmitter release mechanisms studied in *Caenorhabditis elegans*. *Cell Calcium* **52,** 289–295 CrossRef Medline
17. Vashlishan, A. B., Madison, J. M., Dybbs, M., Bai, J., Sieburth, D., Ch'ng, Q., Tavazoie, M., and Kaplan, J. M. (2008) An RNAi screen identifies genes that regulate GABA synapses. *Neuron* **58,** 346–361 CrossRef Medline
18. Sun, Y., Hu, Z., Goeb, Y., and Dreier, L. (2013) The F-box protein MEC-15 (FBXW9) promotes synaptic transmission in GABAergic motor neurons in *C. elegans*. *PLoS One* **8,** e59132 CrossRef Medline
19. Kowalski, J. R., Dube, H., Touroutine, D., Rush, K. M., Goodwin, P. R., Carozza, M., Didier, Z., Francis, M. M., and Juo, P. (2014) The anaphase-promoting complex (APC) ubiquitin ligase regulates GABA transmission at the *C. elegans* neuromuscular junction. *Mol. Cell Neurosci.* **58,** 62–75 CrossRef Medline
20. Opperman, K. J., Mulcahy, B., Giles, A. C., Risley, M. G., Birnbaum, R. L., Tulgren, E. D., Dawson-Scully, K., Zhen, M., and Grill, B. (2017) The HECT family ubiquitin ligase EEL-1 regulates neuronal function and development. *Cell Rep.* **19,** 822–835 CrossRef Medline
21. Orivoli, S., Pavlidis, E., Cantalupo, G., Pezzella, M., Zara, F., Garavelli, L., Pisani, F., and Piccolo, B. (2016) Xp11.22 microduplications including HUWE1: case report and literature review. *Neuropediatrics* **47,** 51–56 Medline
22. Moortgat, S., Berland, S., Aukrust, I., Maystadt, I., Baker, L., Benoit, V., Caro-Llopis, A., Cooper, N. S., Debray, F. G., Faivre, L., Gardeitchik, T., Haukanes, B. I., Houge, G., Kivuva, E., Martinez, F., *et al.* (2018) HUWE1 variants cause dominant X-linked intellectual disability: a clinical study of 21 patients. *Eur. J. Hum. Genet.* **26,** 64–74 CrossRef Medline
23. Friez, M. J., Brooks, S. S., Stevenson, R. E., Field, M., Basehore, M. J., Adès, L. C., Sebold, C., McGee, S., Saxon, S., Skinner, C., Craig, M. E., Murray, L., Simensen, R. J., Yap, Y. Y., Shaw, M. A., *et al.* (2016) HUWE1 mutations in Juberg-Marsidi and Brooks syndromes: the results of an X-chromosome exome sequencing study. *BMJ Open* **6,** e009537 CrossRef Medline
24. Kreppel, L. K., Blomberg, M. A., and Hart, G. W. (1997) Dynamic glycosylation of nuclear and cytosolic proteins: cloning and characterization of a unique *O*-GlcNAc transferase with multiple tetratricopeptide repeats. *J. Biol. Chem.* **272,** 9308–9315 CrossRef Medline
25. Levine, Z. G., and Walker, S. (2016) The biochemistry of *O*-GlcNAc transferase: which functions make it essential in mammalian cells? *Annu. Rev. Biochem.* **85,** 631–657 CrossRef Medline
26. Hart, G. W. (2019) Nutrient regulation of signaling and transcription. *J. Biol. Chem.* **294,** 2211–2231 CrossRef Medline
27. Cole, R. N., and Hart, G. W. (2001) Cytosolic *O*-glycosylation is abundant in nerve terminals. *J. Neurochem.* **79,** 1080–1089 Medline
28. Akimoto, Y., Comer, F. I., Cole, R. N., Kudo, A., Kawakami, H., Hirano, H., and Hart, G. W. (2003) Localization of the *O*-GlcNAc transferase and *O*-GlcNAc-modified proteins in rat cerebellar cortex. *Brain Res.* **966,** 194–205 CrossRef Medline
29. Vosseller, K., Trinidad, J. C., Chalkley, R. J., Specht, C. G., Thalhammer, A., Lynn, A. J., Snedecor, J. O., Guan, S., Medzihradszky, K. F., Maltby, D. A., Schoepfer, R., and Burlingame, A. L. (2006) *O*-linked *N*-acetylglucosamine proteomics of postsynaptic density preparations using lectin weak affinity chromatography and mass spectrometry. *Mol. Cell. Proteomics* **5,** 923–934 CrossRef Medline
30. Pekkurnaz, G., Trinidad, J. C., Wang, X., Kong, D., and Schwarz, T. L. (2014) Glucose regulates mitochondrial motility via Milton modification by *O*-GlcNAc transferase. *Cell* **158,** 54–68 CrossRef Medline
31. Wani, W. Y., Chatham, J. C., Darley-Usmar, V., McMahon, L. L., and Zhang, J. (2017) *O*-GlcNAcylation and neurodegeneration. *Brain Res. Bull.* **133,** 80–87 CrossRef Medline
32. Ruan, H. B., Dietrich, M. O., Liu, Z. W., Zimmer, M. R., Li, M. D., Singh, J. P., Zhang, K., Yin, R., Wu, J., Horvath, T. L., and Yang, X. (2014) *O*-GlcNAc transferase enables AgRP neurons to suppress browning of white fat. *Cell* **159,** 306–317 CrossRef Medline
33. Lagerlöf, O., Slocomb, J. E., Hong, I., Aponte, Y., Blackshaw, S., Hart, G. W., and Huganir, R. L. (2016) The nutrient sensor OGT in PVN neurons regulates feeding. *Science* **351,** 1293–1296 CrossRef Medline
34. Mahoney, T. R., Luo, S., and Nonet, M. L. (2006) Analysis of synaptic transmission in *Caenorhabditis elegans* using an aldicarb-sensitivity assay. *Nat. Protoc.* **1,** 1772–1777 CrossRef Medline
35. Ramot, D., Johnson, B. E., Berry, T. L., Jr, Carnell, L., and Goodman, M. B. (2008) The Parallel Worm Tracker: a platform for measuring average speed and drug-induced paralysis in nematodes. *PLoS One* **3,** e2208 CrossRef Medline

36. Wang, Z. W., Saifee, O., Nonet, M. L., and Salkoff, L. (2001) SLO-1 potassium channels control quantal content of neurotransmitter release at the C. elegans neuromuscular junction. *Neuron* **32,** 867–881 CrossRef Medline
37. Zhao, X., Heng, J. I., Guardavaccaro, D., Jiang, R., Pagano, M., Guillemot, F., Iavarone, A., and Lasorella, A. (2008) The HECT-domain ubiquitin ligase Huwe1 controls neural differentiation and proliferation by destabilizing the N-Myc oncoprotein. *Nat. Cell Biol.* **10,** 643–653 CrossRef Medline
38. Rotin, D., and Kumar, S. (2009) Physiological functions of the HECT family of ubiquitin ligases. *Nat. Rev. Mol. Cell Biol.* **10,** 398–409 CrossRef Medline
39. de Groot, R. E., Ganji, R. S., Bernatik, O., Lloyd-Lewis, B., Seipel, K., Šedová, K., Zdráhal, Z., Dhople, V. M., Dale, T. C., Korswagen, H. C., and Bryja, V. (2014) Huwe1-mediated ubiquitylation of dishevelled defines a negative feedback loop in the Wnt signaling pathway. *Sci. Signal.* **7,** ra26 CrossRef Medline
40. Forget, A., Bihannic, L., Cigna, S. M., Lefevre, C., Remke, M., Barnat, M., Dodier, S., Shirvani, H., Mercier, A., Mensah, A., Garcia, M., Humbert, S., Taylor, M. D., Lasorella, A., and Ayrault, O. (2014) Shh signaling protects Atoh1 from degradation mediated by the E3 ubiquitin ligase Huwe1 in neural precursors. *Dev. Cell* **29,** 649–661 CrossRef Medline
41. Urbán, N., van den Berg, D. L., Forget, A., Andersen, J., Demmers, J. A., Hunt, C., Ayrault, O., and Guillemot, F. (2016) Return to quiescence of mouse neural stem cells by degradation of a proactivation protein. *Science* **353,** 292–295 CrossRef Medline
42. Yin, L., Joshi, S., Wu, N., Tong, X., and Lazar, M. A. (2010) E3 ligases Arf-bp1 and Pam mediate lithium-stimulated degradation of the circadian heme receptor Rev-erb α. *Proc. Natl. Acad. Sci. U.S.A.* **107,** 11614–11619 CrossRef Medline
43. Vaughan, L., Tan, C. T., Chapman, A., Nonaka, D., Mack, N. A., Smith, D., Booton, R., Hurlstone, A. F., and Malliri, A. (2015) HUWE1 ubiquitylates and degrades the RAC activator TIAM1 promoting cell-cell adhesion disassembly, migration, and invasion. *Cell Rep.* **10,** 88–102 CrossRef Medline
44. Guo, B., Liang, Q., Li, L., Hu, Z., Wu, F., Zhang, P., Ma, Y., Zhao, B., Kovács, A. L., Zhang, Z., Feng, D., Chen, S., and Zhang, H. (2014) *O*-GlcNAc-modification of SNAP-29 regulates autophagosome maturation. *Nat. Cell Biol.* **16,** 1215–1226 CrossRef Medline
45. Hanover, J. A., Forsythe, M. E., Hennessey, P. T., Brodigan, T. M., Love, D. C., Ashwell, G., and Krause, M. (2005) A *Caenorhabditis elegans* model of insulin resistance: altered macronutrient storage and dauer formation in an OGT-1 knockout. *Proc. Natl. Acad. Sci. U.S.A.* **102,** 11266–11271 CrossRef Medline
46. Love, D. C., Ghosh, S., Mondoux, M. A., Fukushige, T., Wang, P., Wilson, M. A., Iser, W. B., Wolkow, C. A., Krause, M. W., and Hanover, J. A. (2010) Dynamic *O*-GlcNAc cycling at promoters of *Caenorhabditis elegans* genes regulating longevity, stress, and immunity. *Proc. Natl. Acad. Sci. U.S.A.* **107,** 7413–7418 CrossRef Medline
47. Lazarus, M. B., Nam, Y., Jiang, J., Sliz, P., and Walker, S. (2011) Structure of human *O*-GlcNAc transferase and its complex with a peptide substrate. *Nature* **469,** 564–567 CrossRef Medline
48. Schimpl, M., Zheng, X., Borodkin, V. S., Blair, D. E., Ferenbach, A. T., Schüttelkopf, A. W., Navratilova, I., Aristotelous, T., Albarbarawi, O., Robinson, D. A., Macnaughtan, M. A., and van Aalten, D. M. (2012) *O*-GlcNAc transferase invokes nucleotide sugar pyrophosphate participation in catalysis. *Nat. Chem. Biol.* **8,** 969–974 CrossRef Medline
49. Mariappa, D., Zheng, X., Schimpl, M., Raimi, O., Ferenbach, A. T., Müller, H. A., and van Aalten, D. M. (2015) Dual functionality of *O*-GlcNAc transferase is required for *Drosophila* development. *Open Biol.* **5,** 150234 CrossRef Medline
50. Yang, X., Zhang, F., and Kudlow, J. E. (2002) Recruitment of *O*-GlcNAc transferase to promoters by corepressor mSin3A: coupling protein *O*-GlcNAcylation to transcriptional repression. *Cell* **110,** 69–80 CrossRef Medline
51. Ruan, H. B., Han, X., Li, M. D., Singh, J. P., Qian, K., Azarhoush, S., Zhao, L., Bennett, A. M., Samuel, V. T., Wu, J., Yates, J. R., 3rd, Yang, X. (2012) *O*-GlcNAc transferase/host cell factor C1 complex regulates gluconeogenesis by modulating PGC-1alpha stability. *Cell Metab.* **16,** 226–237 CrossRef Medline
52. Hein, M. Y., Hubner, N. C., Poser, I., Cox, J., Nagaraj, N., Toyoda, Y., Gak, I. A., Weisswange, I., Mansfeld, J., Buchholz, F., Hyman, A. A., and Mann, M. (2015) A human interactome in three quantitative dimensions organized by stoichiometries and abundances. *Cell* **163,** 712–723 CrossRef Medline
53. Singh, J. P., Zhang, K., Wu, J., and Yang, X. (2015) *O*-GlcNAc signaling in cancer metabolism and epigenetics. *Cancer Lett.* **356,** 244–250 CrossRef Medline
54. Bernassola, F., Karin, M., Ciechanover, A., and Melino, G. (2008) The HECT family of E3 ubiquitin ligases: multiple players in cancer development. *Cancer Cell* **14,** 10–21 CrossRef Medline
55. Zhao, X., D'Arca, D., Lim, W. K., Brahmachary, M., Carro, M. S., Ludwig, T., Cardo, C. C., Guillemot, F., Aldape, K., Califano, A., Iavarone, A., and Lasorella, A. (2009) The N-Myc-DLL3 cascade is suppressed by the ubiquitin ligase Huwe1 to inhibit proliferation and promote neurogenesis in the developing brain. *Dev. Cell* **17,** 210–221 CrossRef Medline
56. Andres, L. M., Blong, I. W., Evans, A. C., Rumachik, N. G., Yamaguchi, T., Pham, N. D., Thompson, P., Kohler, J. J., and Bertozzi, C. R. (2017) Chemical modulation of protein *O*-GlcNAcylation via OGT inhibition promotes human neural cell differentiation. *ACS Chem. Biol.* **12,** 2030–2039 CrossRef Medline
57. Hu, Y., Suarez, J., Fricovsky, E., Wang, H., Scott, B. T., Trauger, S. A., Han, W., Hu, Y., Oyeleye, M. O., and Dillmann, W. H. (2009) Increased enzymatic *O*-GlcNAcylation of mitochondrial proteins impairs mitochondrial function in cardiac myocytes exposed to high glucose. *J. Biol. Chem.* **284,** 547–555 CrossRef Medline
58. Senyilmaz, D., Virtue, S., Xu, X., Tan, C. Y., Griffin, J. L., Miller, A. K., Vidal-Puig, A., and Teleman, A. A. (2015) Regulation of mitochondrial morphology and function by stearoylation of TFR1. *Nature* **525,** 124–128 CrossRef Medline
59. Leboucher, G. P., Tsai, Y. C., Yang, M., Shaw, K. C., Zhou, M., Veenstra, T. D., Glickman, M. H., and Weissman, A. M. (2012) Stress-induced phosphorylation and proteasomal degradation of mitofusin 2 facilitates mitochondrial fragmentation and apoptosis. *Mol Cell* **47,** 547–557 CrossRef Medline
60. Vaidyanathan, K., Niranjan, T., Selvan, N., Teo, C. F., May, M., Patel, S., Weatherly, B., Skinner, C., Opitz, J., Carey, J., Viskochil, D., Gecz, J., Shaw, M., Peng, Y., Alexov, E., *et al.* (2017) Identification and characterization of a missense mutation in the *O*-linked β-*N*-acetylglucosamine (*O*-GlcNAc) transferase gene that segregates with X-linked intellectual disability. *J. Biol. Chem.* **292,** 8948–8963 CrossRef Medline
61. Willems, A. P., Gundogdu, M., Kempers, M. J. E., Giltay, J. C., Pfundt, R., Elferink, M., Loza, B. F., Fuijkschot, J., Ferenbach, A. T., van Gassen, K. L. I., van Aalten, D. M. F., and Lefeber, D. J. (2017) Mutations in *N*-acetylglucosamine (*O*-GlcNAc) transferase in patients with X-linked intellectual disability. *J. Biol. Chem.* **292,** 12621–12631 CrossRef Medline
62. Brenner, S. (1974) The genetics of *Caenorhabditis elegans*. *Genetics* **77,** 71–94 Medline
63. Mello, C. C., Kramer, J. M., Stinchcomb, D., and Ambros, V. (1991) Efficient gene transfer in *C. elegans*: extrachromosomal maintenance and integration of transforming sequences. *EMBO J.* **10,** 3959–3970 CrossRef Medline
64. Frøkjaer-Jensen, C., Davis, M. W., Hopkins, C. E., Newman, B. J., Thummel, J. M., Olesen, S. P., Grunnet, M., and Jorgensen, E. M. (2008) Single-copy insertion of transgenes in *Caenorhabditis elegans*. *Nat. Genet.* **40,** 1375–1383 CrossRef Medline
65. Swierczek, N. A., Giles, A. C., Rankin, C. H., and Kerr, R. A. (2011) High-throughput behavioral analysis in *C. elegans*. *Nat. Methods* **8,** 592–598 CrossRef Medline
66. Stiernagle, T. (2006) Maintenance of *C. elegans*. *WormBook*, 1–11 CrossRef Medline
67. Nesvizhskii, A. I., Keller, A., Kolker, E., and Aebersold, R. (2003) A statistical model for identifying proteins by tandem mass spectrometry. *Anal. Chem.* **75,** 4646–4658 CrossRef Medline